Electronic Supplementary Material (ESI) for ChemComm.

Supporting Information

Capturing Neon – The First Experimental Structure of Neon Trapped Within a Metal-Organic Environment

Peter A. Wood, Amy A. Sarjeant, Andrey A. Yakovenko, Suzanna C. Ward,
Colin R. Groom

Correspondence to: wood@ccdc.cam.ac.uk

This document includes:

Materials and Methods
Figs. S1 to S12
Tabs. S1 to S2
Additional References

Materials and Methods

In situ synchrotron powder diffraction data collection

In situ high-gas pressure diffraction data in a neon atmosphere were collected using the monochromatic X-rays available at the 17-BM (0.72768 Å) beamline (300 μm diameter beam size) at the Advanced Photon Source, Argonne National Laboratory in combination with a Perkin-Elmer amorphous-Si flat panel detector. Each MOF sample was loaded into a 1.0 mm Kapton capillary with glass wool on either side. The capillary was then loaded into the gas flow-cell (*21*), with a thermocouple inserted just at the edge of the packed sample, to perform *in situ* PXRD experiments. At one end the gas cell was connected to a two-way valve which allowed changing between a 1 atm helium flow and a high pressure syringe pump (Teledyne ISCO 500D) which was filled with neon gas. The measurement procedure included several steps as outlined below.

Activation of MOF samples

The crystalline samples of PCN-200 and NiMOF-74 were kindly provided by Dr Mario Wriedt (Clarkson University) and Dr Hongcai Zhou (Texas A&M University), respectively. Ultra-high purity (UHP) neon gas was supplied by Airgas.

Activation procedures for both PCN-200 and NiMOF-74 for *in situ* powder diffraction measurements have been established previously and very similar conditions were used for this experiment as those described before (*14, 20, 22*). Furnace elements were bolted onto the gas cell above and below the capillary and computer controlled throughout the process of MOF activation. Helium gas was allowed to flow through the capillary and sample at 10 mL/min. Meanwhile, the temperature was ramped from ambient temperature (approximately 295 K) to 373 K for PCN-200 and to 498 K for NiMOF-74 at 20 K/min. In the case of PCN-200 we heated the sample at the activation temperature for 5 minutes and then cooled down to room temperature, while in the case of NiMOF-74 the sample was held at the activation temperature for more than 6 hours.

During the course of activation of PCN-200, the phase change corresponding to water loss from the pores of the PCN-200 was clearly observed (Fig. S1). This was used as an indicator of a successful activation procedure (*14, 22*). NiMOF-74 does not undergo a phase change upon activation and no shifting of the diffraction pattern was observed. However, the following Rietveld analysis of the heated sample confirmed that there is no major difference electron density (ρ_{max}/ρ_{min} = 0.06/-0.08 eÅ-3) present in the pores (Fig. S2).

Neon gas loading experiments

After activation of each MOF sample, the gas flow cell was connected to the syringe pump and helium gas in the capillary was exchanged with a neon flow for 10 minutes. The furnace elements were removed, and the Oxford Cryosystems Cryostream 700 plus was installed above the capillary. The flow-cell/syringe pump system was sealed and neon gas pressure was increased to 5 bar. The temperature and pressure of the sample was computer controlled during the entire gas loading experiment. Powder diffraction images were recorded at increments of 5 bar, while the gas pressure was raised from 5 bar to 100 bar and then released back to 5 bar. This pressure cycle and PXRD data collection was performed for both PCN-200 and NiMOF-74 at three different temperatures 295K, 200K and 100K.

Data Processing

The raw images were processed within GSAS-II (*24*), refining the sample-to-detector distance and tilt of the detector relative to the beam based on data obtained for a LaB_6 standard (*24*). Collected and integrated *in situ* powder diffraction data sets were trimmed, normalized and plotted using 2DFLT software (*25*) (Figs. S3 and S4). There was no significant peak position change during the neon loading and unloading processes at all temperatures, indicating that there was no crystallographic phase transition. At the same time it was evident that relative peak intensities in patterns were changing slightly corresponding to the incorporation of Ne atoms into the crystallographic lattice.

In the case of the PCN-200 experiment at 100 K we also noticed the appearance of new peaks (near $2\theta = 3°$) towards the end of the pressure cycle corresponding to the non-activated phase of the MOF (Fig. S3). This indicates some small air exposure of the system at 100 K temperature during depressurization. We did not observe the same effect in case of the 295 K or 200 K experiments, however in our structure analysis we have excluded data from the depressurization half-cycle for all PCN-200 samples.

Details for the Rietveld refinements

The unit cell dimensions, the relative intensities of peaks and the structural parameters of the MOFs were evaluated by Rietveld fits to the diffraction data within JANA2006 (*25*). The Rietveld refinement was performed for the pattern corresponding to 100 bar neon pressure in each data set (patterns #19 on Figs. S3 and S4), using unit cell and structural parameters for PCN-200 and NiMOF-74 found previously (*21*, *14*). These initial refinements were performed using the empty MOF framework coordinates only. These initial refinements studies were performed for the purpose of difference Fourier map generation.

The bond lengths and angles for the organic ligands were assumed to be minimally effected by neon pressure and were refined as a combination of rigid bodies and multiple bond length and bond angle parameters. The isotropic atomic displacement parameters of the light atoms (carbon, nitrogen, oxygen) in the organic ligand moieties were set to be equal and subsequently refined. In case of NiMOF-74 refinements, the isotropic atomic displacement parameter of the nickel atom was also coupled with U_{iso} of light atoms. After the best refinement parameters were reached, F_{obs} - F_{calc} densities were calculated and corresponding maps were plotted using the VESTA (*27*) software package (Figs. S5 and S6). After determination of the Ne atom positions from difference density maps, Ne atoms were introduced into a structural model. Positions and occupancies of the Ne atoms were refined freely, but the isotropic displacement parameters were set to be three times that of the U_{iso} of the ligand atoms. Crystal data and structure refinement parameters for 100 bar neon pressure patterns (number 19 on Figs. S3 and S4) are reported in Tables S1 and S2. The final Rietveld plots for these patterns are reported in Figs. S7 and S8.

After satisfactory refinement parameters were reached, patterns with numbers from 18 to 1 for PCN-200 (Fig. S3) and from 18 to 1 and 20 to 39 for NiMOF-74 (Fig. S4) were refined sequentially. The quality of the refinement was monitored by comparing R_p, R_{wp} and *GOF* (Figs. S9 and S10).

In the case of the PCN-200 refinements for the 200 K and 100 K experiments it was found that Ne occupancies were not refining to convergence and produced unreasonable results. In these cases we sequentially re-refined the data using the structural model of the empty MOF and then calculated F_{obs}- F_{calc} densities for each pressure step. From these densities we found values of difference densities $\Delta\rho_{max}$ at the Ne1 and Ne2 positions. After plotting their ratio ($\Delta\rho_{max}$(Ne2)/$\Delta\rho_{max}$(Ne1)) *vs* pressure we found that the ratio has a very linear dependence (Fig. S11). We assumed that the $\Delta\rho_{max}$ ratio should be equal to the ratio of the Ne atom occupancies (*n*) at each position, as represented by the equation below:

$$\frac{n(Ne2)}{n(Ne1)} = \frac{\Delta\rho_{max}(Ne2)}{\Delta\rho_{max}(Ne1)}$$

Hence, in our final sequential refinements of the 100 K and 200 K experimental data for PCN-200 we used following equation to calculate occupancy at Ne2 position:

$$n(Ne2) = (kP + b)n(Ne1)$$

where *P* is the neon gas pressure in bar, *k* and *b* are linear fit coefficients in accordance with Fig. S11.

Structure analysis

Crystal structures were visualized and analyzed using the program Mercury version 3.8 (*28*) and the same software was used in combination with POV-Ray (*29*) for the generation of structural figures throughout.

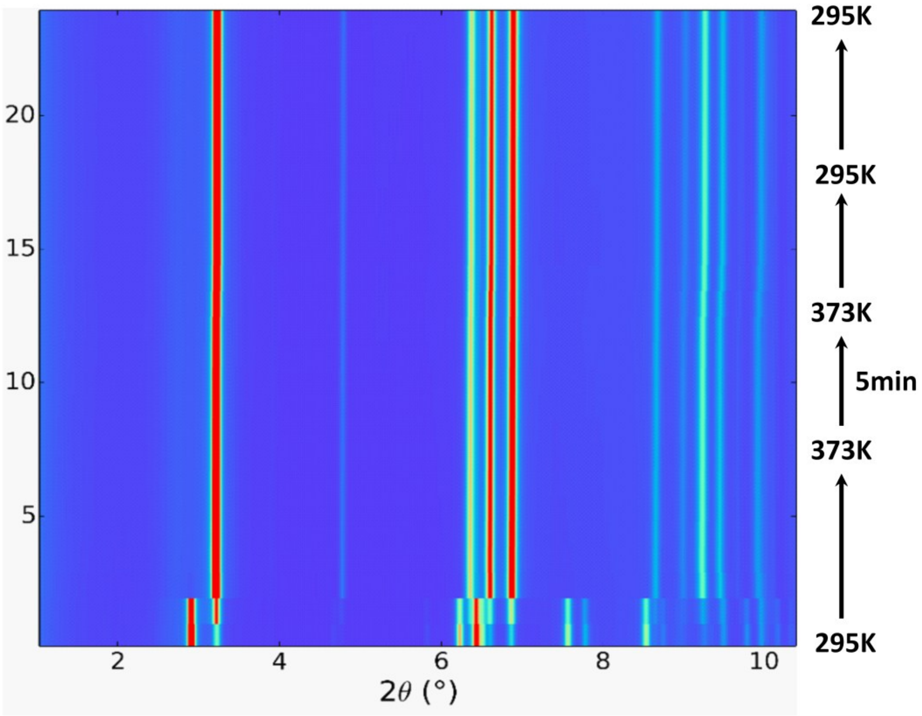

Fig. S1. PXRD data illustrating the activation of the PCN-200 sample. The temperature was increased from 295 K to 373 K at a rate of 20 K/min with powder diffraction images collected every 60 seconds. The water in the MOF pores is lost in the first 4 minutes, illustrated by the shifting of peaks associated with a phase change.

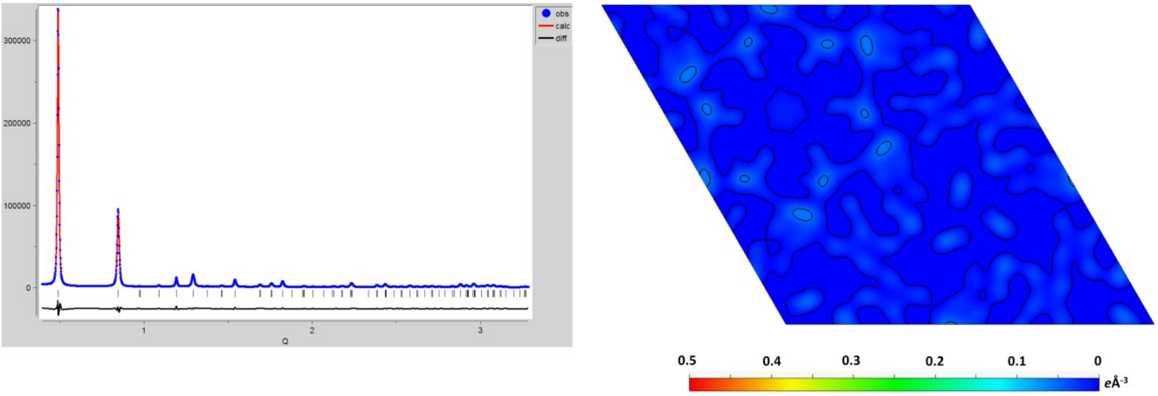

(a)

(b)

Fig. S2. (a) Final Rietveld refinement plot of NiMOF-74 sample PXRD data collected after 3 hours of activation in helium flow at 498K. (*Rp* = 4.05% *Rwp* = 5.62% GOF=3.80) and (b) Fourier difference density plot calculated from results of this refinement and drawn in the (006) crystallographic plane.

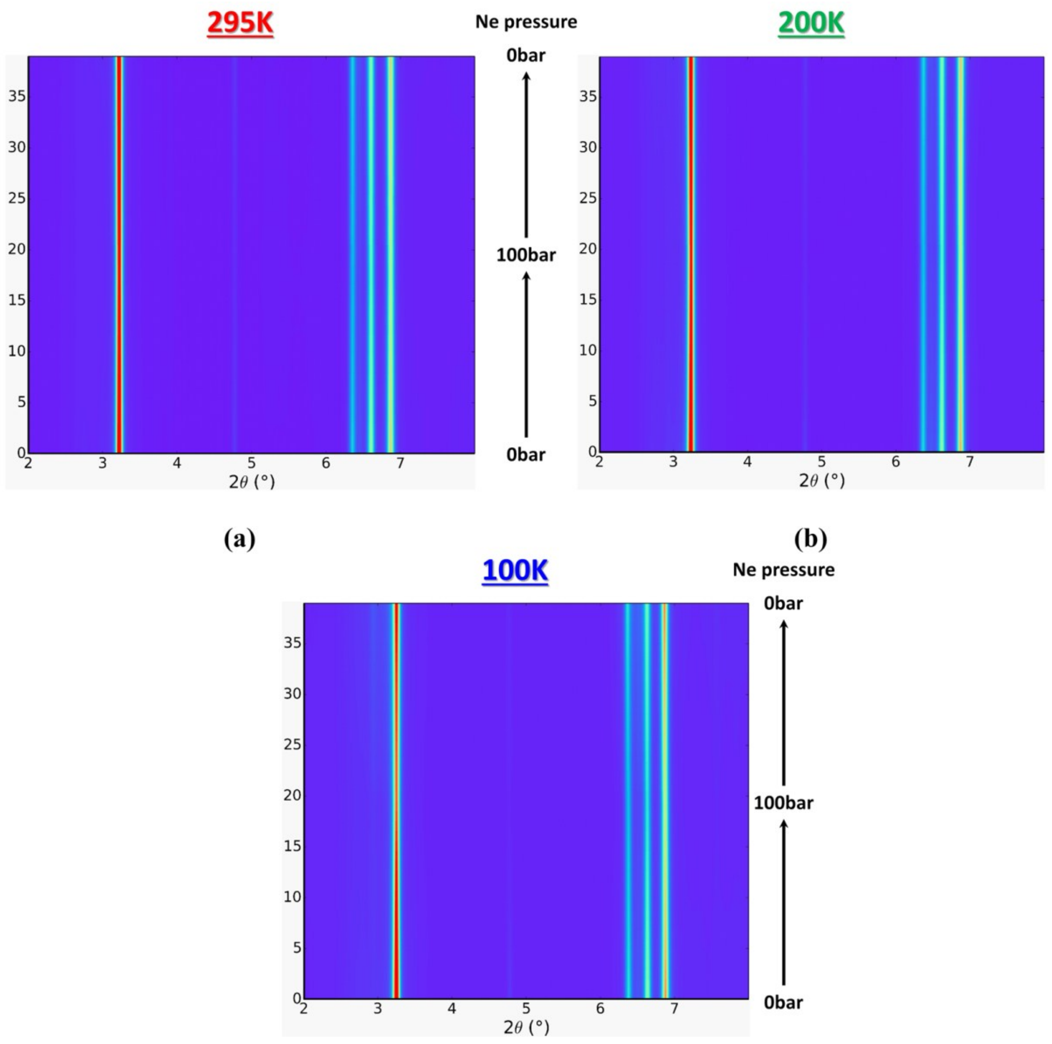

(a) (b)

(c)

Fig. S3. Top view of the powder diffraction patterns for PCN-200 from the *in situ* high-pressure neon loading experiments. Upon increase or release of the pressure at 295K and 200K, no crystallographic phase transitions were observed. However, in the case of the 100 K experiment appearance of small peaks corresponding to the hydrated form of PCN-200 were observed during depressurization (near 2θ = 3°).

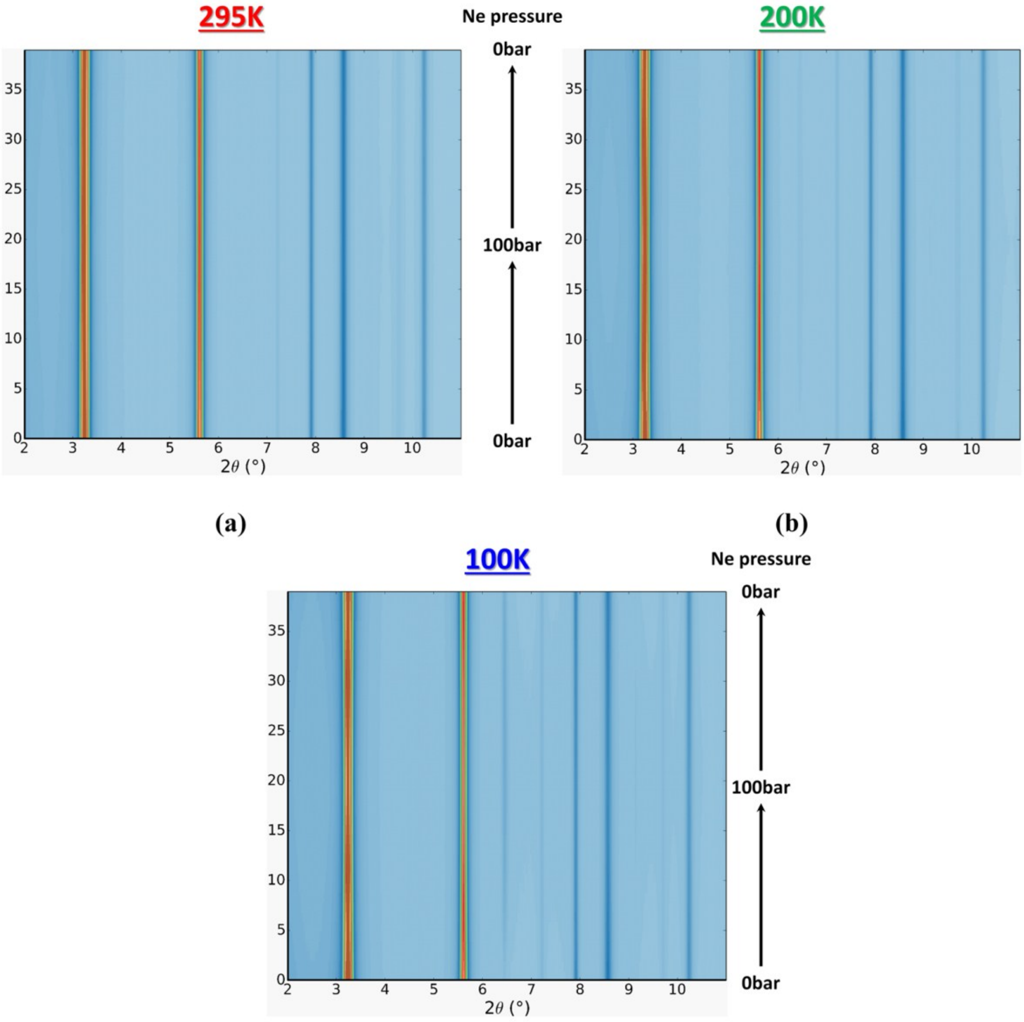

(a) (b)

(c)

Fig. S4. Top view of the powder diffraction patterns for NiMOF-74 from the *in situ* high-pressure neon loading experiments. Upon increase or release of the pressure, no crystallographic phase transitions were observed.

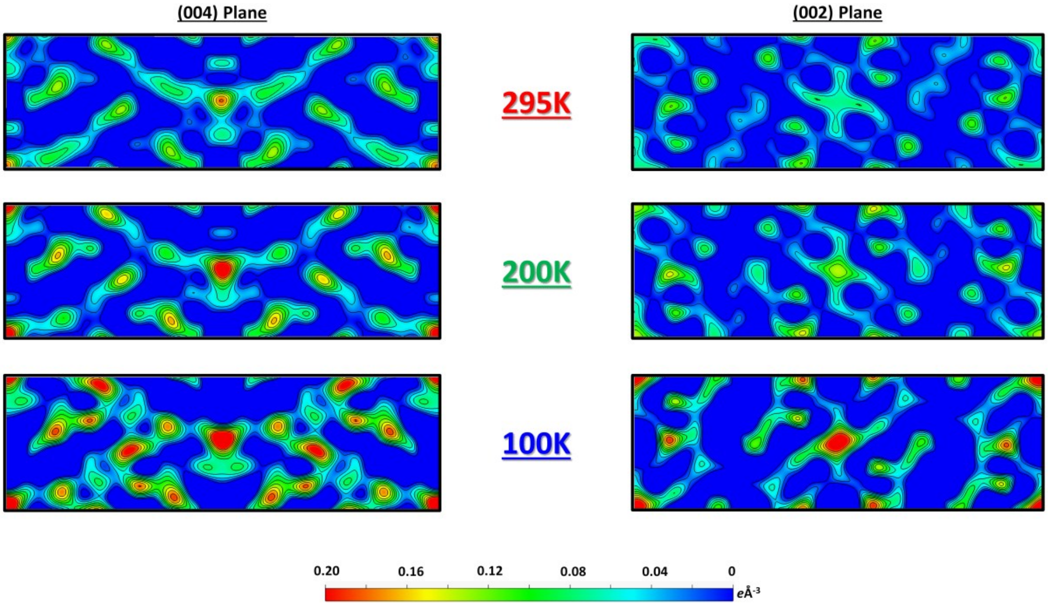

Fig. S5. Fourier difference density maps in the (004) and (002) planes for PCN-200 at neon positions for Ne1 (0.5; 0.5; 0.25) and Ne2 (0.5; 0.5; 0.5), respectively, showing the relative residual electron density at each site at 100 bar of neon pressure. The very low value for Ne2 at 295 K indicates that there is no neon present in this site at this temperature.

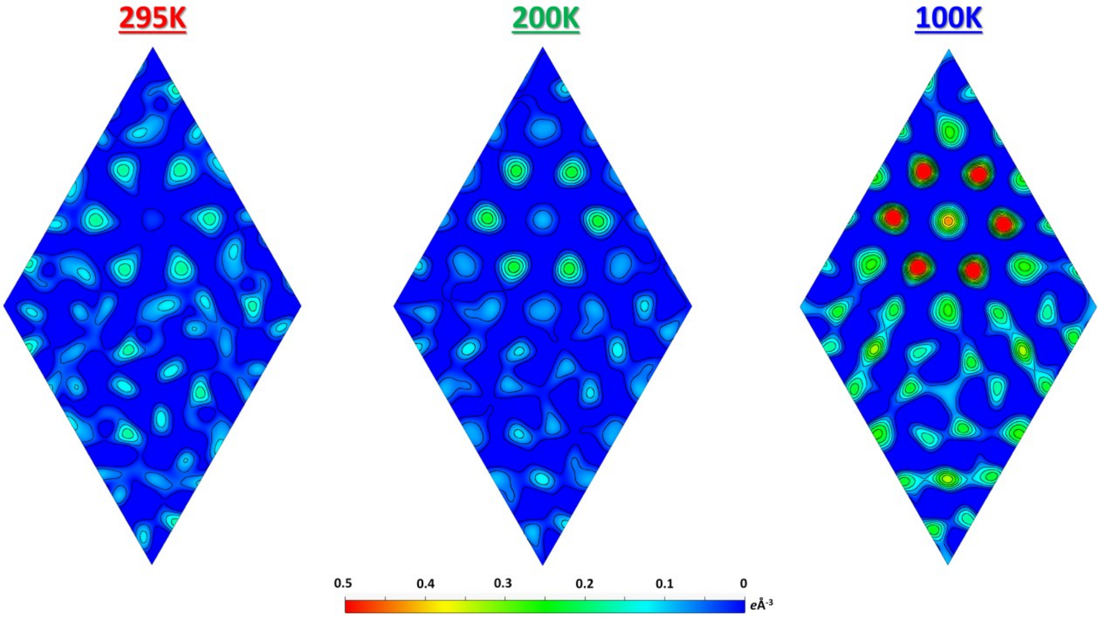

Fig. S6. Fourier difference density maps in the (006) plane for NiMOF-74 at each neon position Ne1 (near Ni-atom), Ne2 (in the middle of the pore) showing the relative residual electron density at each site at 100 bar of neon pressure. The very low value for Ne2 at 295 K indicates that there is no neon present in this site at this temperature.

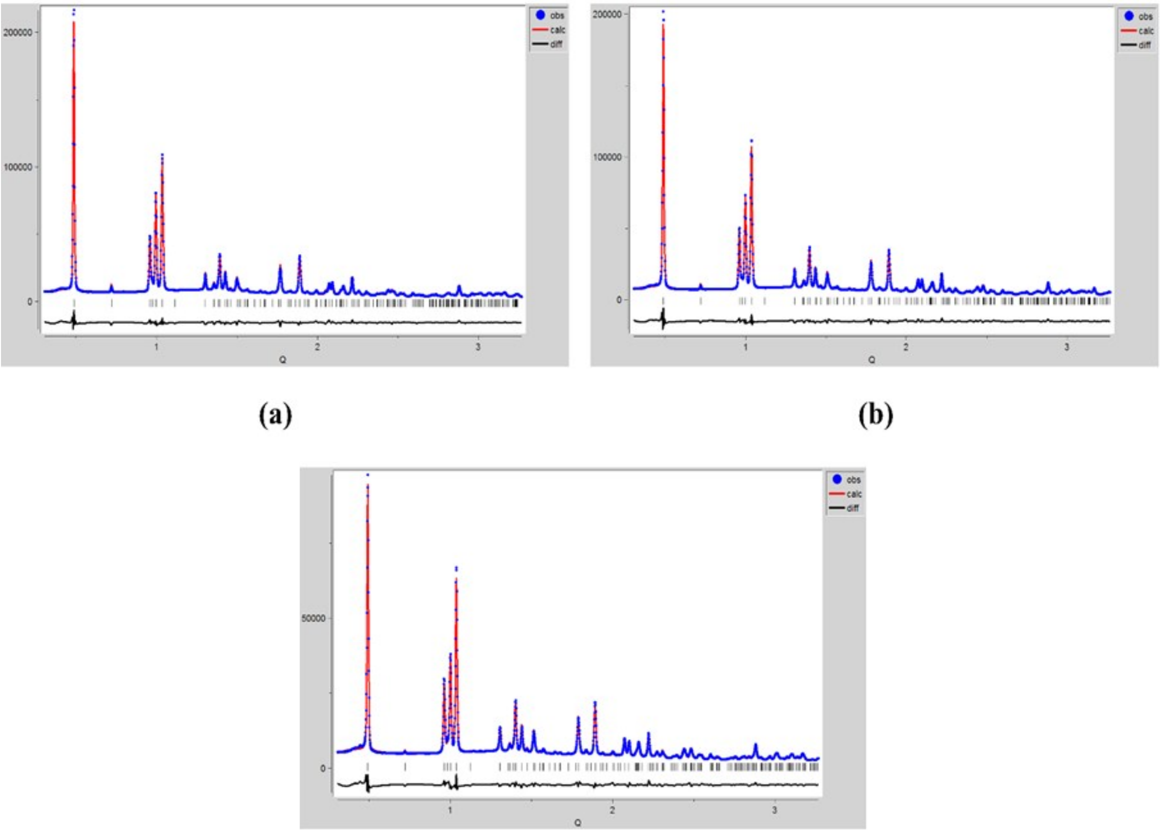

(a)

(b)

(c)

Fig. S7. Final Rietveld refinement plots and difference profiles for the PCN-200 100 bar neon pressure data sets collected at (a) 295 K, (b) 200 K and (c) 100 K

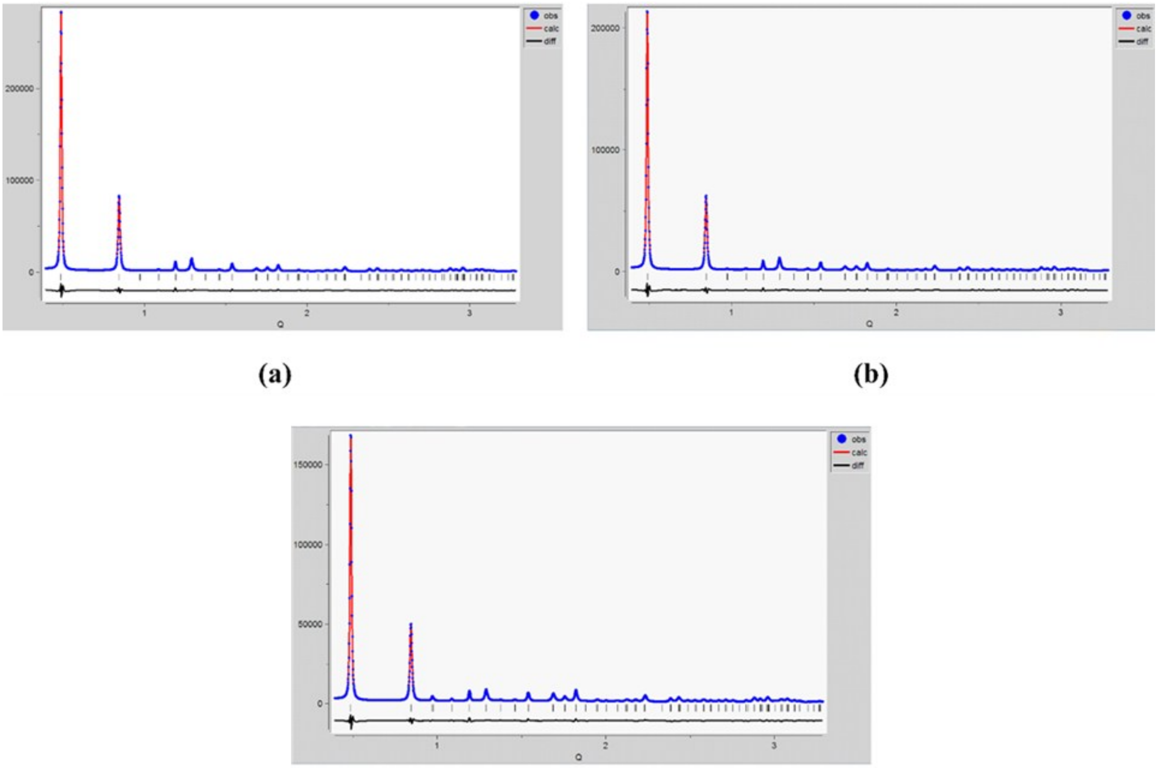

(a)

(b)

(c)

Fig. S8. Final Rietveld refinement plots and difference profiles for the NiMOF-74 100 bar neon pressure data sets collected at (a) 295 K, (b) 200 K and (c) 100 K

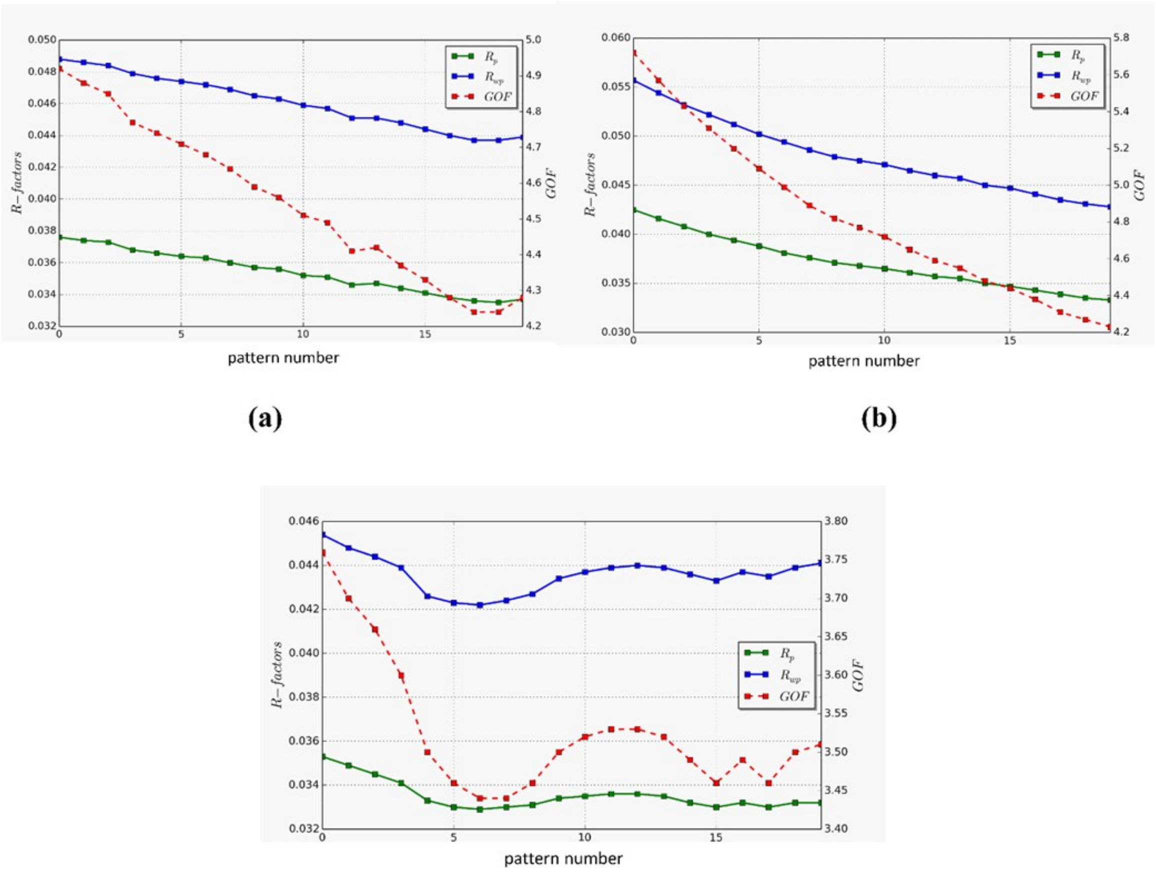

(a) (b)

(c)

Fig. S9. Sequential Rietveld refinement parameters R_p, R_wp and *GOF* plotted *vs* pattern number (see Fig. S3) for the PCN-200 neon gas high pressure diffraction data collected at (a) 295 K, (b) 200 K and (c) 100 K

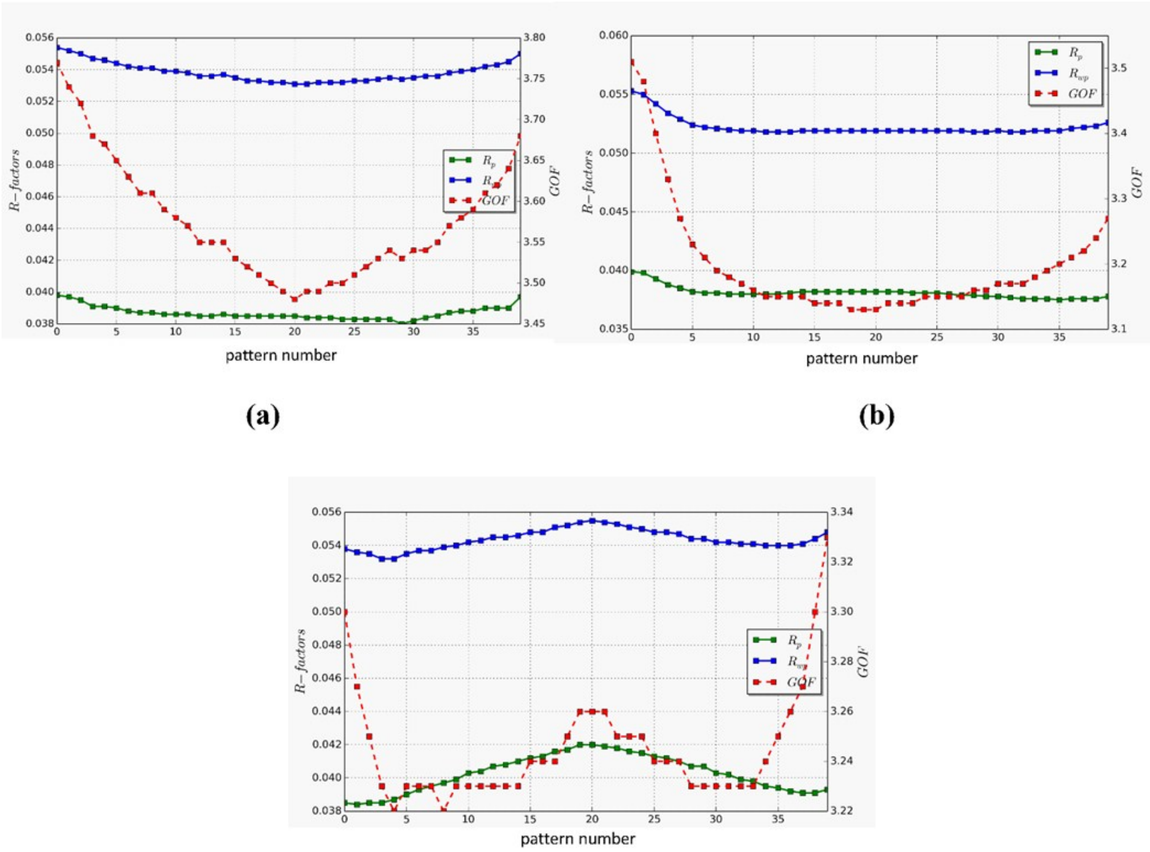

(a) **(b)**

(c)

Fig. S10. Sequential Rietveld refinement parameters R_p, R_wp and *GOF* plotted *vs* pattern number (see Fig. S4) for the NiMOF-74 neon gas high pressure diffraction data collected at (a) 295 K, (b) 200 K and (c) 100 K

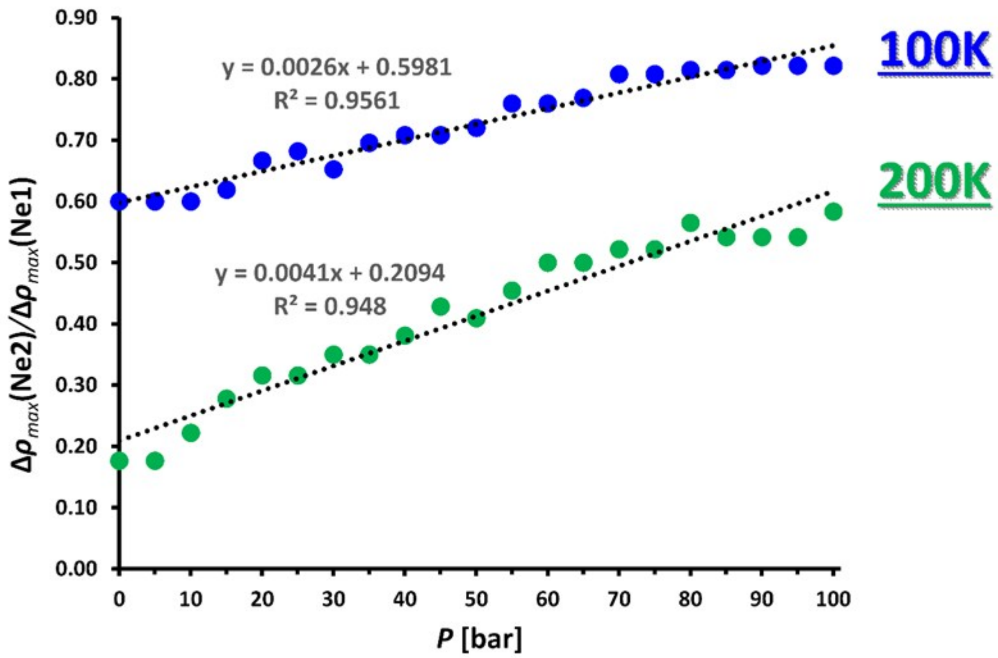

Fig. S11. Pressure dependence of ratios of difference density Δ***ρ***$_{max}$ values at the Ne1 and Ne2 positions in the structure of PCN-200 at 200 K and 100 K. It can be noted that these values closely follow a linear trend.

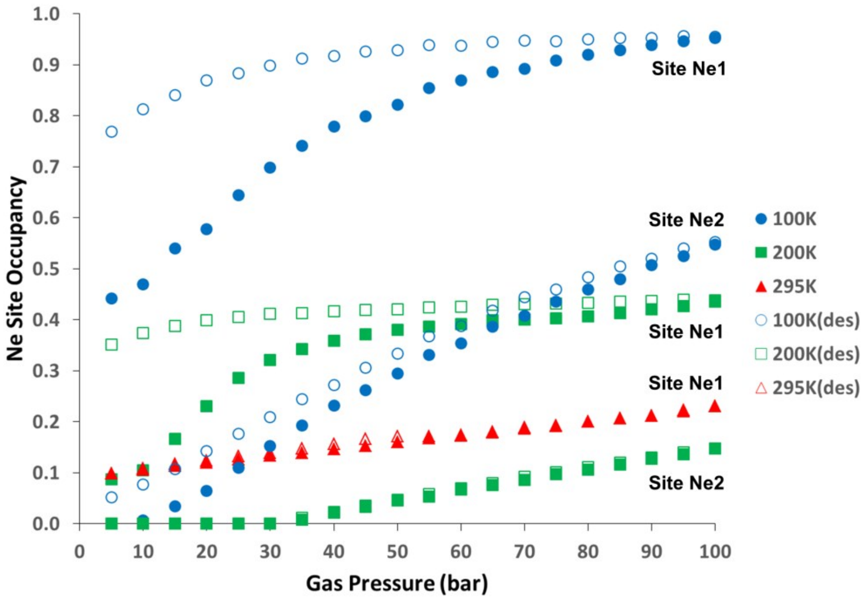

Fig. S12. Graph of neon site occupancies within NiMOF-74 as a function of gas pressure upon adsorption (filled symbols) and desorption (open symbols) at 295 K (triangles), 200 K (squares) and 100 K (circles). Note that only site Ne1 is filled in NiMOF-74 at 295 K.

Tab. S1. Refinement and crystal structure details from Rietveld fits for PCN-200 at 100 bar of neon pressure.

Temperature (K)	100	200K	295K
Chemical formula	[$Cu_2(C_{17}H_{14}N_{10}O_4)$ 0.892(Ne)]n	[$Cu_2(C_{17}H_{14}N_{10}O_4)$ 0.632(Ne)]n	[$Cu_2(C_{17}H_{14}N_{10}O_4)$ 0.358(Ne)]n
M_r	283.7	281.1	278.3
Crystal system	Monoclinic	Monoclinic	Monoclinic
Space group	*C*2/*c*	*C*2/*c*	*C*2/*c*
a (Å)	28.6315 (13)	28.6841 (11)	28.7444 (11)
b (Å)	9.2743 (5)	9.2655 (5)	9.2672 (5)
c (Å)	9.2833 (5)	9.3005 (4)	9.3295 (4)
β (°)	116.615 (4)	116.369 (3)	116.097 (3)
V (Å^3)	2203.9 (2)	2214.65 (18)	2231.82 (19)
Z	8	8	8
R_p	0.033	0.033	0.034
R_{wp}	0.044	0.043	0.044
R_{Bragg}	0.0320	0.0315	0.0354
GOF	3.51	4.23	4.28
Ne1 (occupancy)	0.480 (9)	0.391 (9)	0.358 (14)
Ne2 (occupancy)	0.411 (8)	0.242 (6)	

Tab. S2. Refinement and crystal structure details from Rietveld fits for NiMOF-74 at 100 bar of neon pressure.

Temperature (K)	100	200	295
Chemical formula	$[Ni(C_4HO_3)1.045(Ne)]n$	$[Ni(C_4HO_3)0.46(Ne)]n$	$[Ni(C_4HO_3)0.223(Ne)]n$
M_r	176.8	165	160.2
Crystal system	Trigonal	Trigonal	Trigonal
Space group	*R*-3	*R*-3	*R*-3
a (Å)	25.7611 (4)	25.7542 (3)	25.7522 (3)
c (Å)	6.7565 (3)	6.7550 (3)	6.7576 (3)
V (Å^3)	3883.1 (2)	3880.17 (19)	3881.04 (19)
Z	18	18	18
$R_{p,}$	0.042	0.038	0.039
R_{wp}	0.055	0.052	0.053
R_{Bragg}	0.0424	0.0280	0.0217
GOF	3.26	3.13	3.50
Ne1 (occupancy)	0.953 (6)	0.436 (7)	0.223 (6)
Ne2 (occupancy)	0.547 (12)	0.147 (11)	

Additional References

21. P. J. Chupas, K. W. Chapman, C. Kurtz, J. C. Hanson, P. L. Lee, C. P. Grey, *J. Appl. Cryst.*, 2008, **41**, 822-824.
22. M. Wriedt, J. P. Sculley, W. M. Verdegaal, A. A. Yakovenko, H.-C. Zhou, *Chem. Commun.*, 2013, **49**, 9612-9614.
23. B. H. Toby, R. B. Von Dreele, *J. Appl. Cryst.*, 2013, **46**, 544-549.
24. A. P. Hammersley, S. O. Svensson, M. Hanfland, A. N. Fitch, D. Hausermann, *High Pressure Res.*, 1996, **14**, 235-248.
25. A. A. Yakovenko, 2DFLT ver.3.4.3, 2014, Upton, NY, USA: Brookhaven National Laboratory.
26. V. Petricek, M. Dusek, L. Palatinus, *Zeit. Krist.*, 2014, **229**, 345-352.
27. K. Momma, F. Izumi, *J. Appl. Cryst.*, 2011, **44**, 1272-1276.
28. C. F. Macrae, I. J. Bruno, J. A. Chisholm, P. R. Edgington, P. McCabe, E. Pidcock, L. Rodriguez-Monge, R. Taylor, J. van de Streek and P. A. Wood, *J. Appl. Cryst.*, 2008, **41**, 466-470.
29. POV-Ray. POV-Ray: the persistence of vision raytracer, 2009.